# Wave-packet and entanglement dynamics in a non-Hermitian many-body system

Takahiro Orito[1] and Ken-Ichiro Imura[2]

[1]*Graduate School of Advanced Science and Engineering, Hiroshima University, Higashi-Hiroshima 739-8530, Japan*
[2]*Institute of Industrial Science, The University of Tokyo, Kashiwa 277-8574, Japan*

The static and dynamical properties of a one-dimensional quantum system described by a non-Hermitian Hamiltonian of the so-called Hatano-Nelson type; a tight-binding model with asymmetric (or non-reciprocal) hopping, are studied. The static properties of the model have been much studied; the complex spectrum, skin effect and its topological interpretation, etc. Effects of disorder and inter-particle interaction, especially, when they coexist, may be less understood. Here, we will also focus on its dynamical properties and reveal some unique features in the wave-packet and entanglement (entropy) dynamics. For that some latest (original) results based on improved numerics (with this a system of larger system size $L$ becomes accessible) are shown.

**KEYWORDS:** non-Hermitian, localization, topological, entanglement

## 1. Introduction

Quantum mechanics described by a non-Hermitian Hamiltonian attracts much attention recently, showing relevance, especially to low temperature physics. An open quantum system is a typical system described by a non-Hermitian Hamiltonian. Here, we consider the Hatano-Nelson type non-Hermitian Hamiltonian with asymmetric (or non-reciprocal) hopping [see, Eq. (1)]. The original Hatano-Nelson model with onsite random (uncorrelated) potential disorder $W_j \in [-W/2, W/2]$ shows in spite of the one dimensionality of the model [1] a localization-delocalization transition at a finite critical disorder strength $W = W_c$ [2]. Its spectrum under the periodic boundary condition (PBC) shows a complex-real transition also at $W = W_c$. Naturally, the existence of generally a finite imaginary part in its eigenvalues is the hallmark of a non-Hermitian Hamiltonian. The weak disorder regime of the Hatano-Nelson model under the PBC indeed falls on this category, while under the open boundary condition (OBC) the spectrum becomes real. Such a sensitivity to the boundary condition is another peculiarity of a non-Hermitian Hamiltonian, already pointed out in the original work of Hatano and Nelson. The behavior of the corresponding eigen wave functions is also peculiar, showing the so-called non-Hermitian skin effect under the OBC. [3]

Here, in this paper we report on some specific consequences of such peculiar features of a non-Hermitian system in its dynamics, taking also into account the effects of inter-particle interaction.

## 2. Model and its static properties

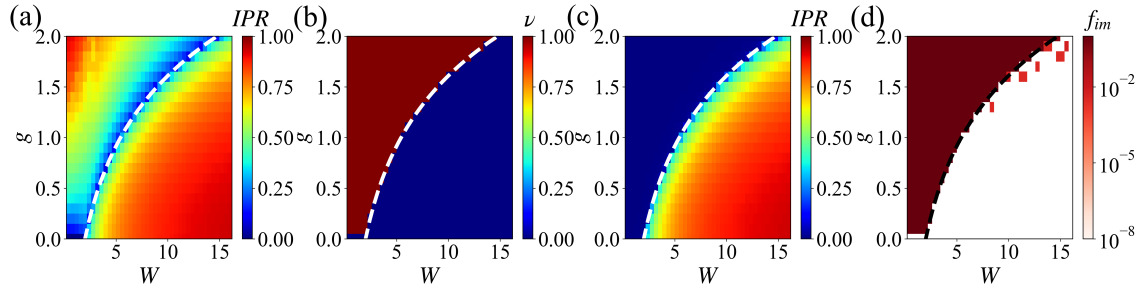Let us consider the following variant of the Hatano-Nelson model:

$$H = \sum_j [-(e^g \hat{c}_j^\dagger \hat{c}_{j+1} + e^{-g} \hat{c}_{j+1}^\dagger \hat{c}_j) + V \hat{n}_j \hat{n}_{j+1} + W_j \hat{n}_j], \qquad (1)$$

where $\hat{c}_j^\dagger$ ($\hat{c}_j$) creates (annihilates) an electron at site $j$, and $\hat{n}_j = \hat{c}_j^\dagger \hat{c}_j$. $g$ is a measure of asymmetry in hopping, while $V$ represents the strength of inter-particle (here, nearest-neighbor) interaction. The last term represents onsite potential disorder at site $j$, which here, we choose to be quasi-periodic; cf.

Aubry-André model [4]:

$$W_j = W \cos(2\pi\theta j + \theta_0), \tag{2}$$

where $\theta$ is an irrational constant and chosen as $\theta = (\sqrt{5} - 1)/2$, and $\theta_0$ is an free parameter to take disorder average. Note that for this type of (correlated) disorder, localization transition occurs at $W = W_c = 2e^g$ in the non-interacting case: $V = 0$, which (in contrast to the original Hatano-Nelson model with uncorrelated disorder) remains finite even in the Hermitian limit: $g = 0$.



**Fig. 1.** A quartet of phase transitions (single-particle case): (a) IPR under OBC, (b) winding number $\nu$, (c) IPR under PBC (d) Im ratio $f_{\text{im}}$ in the space of parameters $(W, g)$.
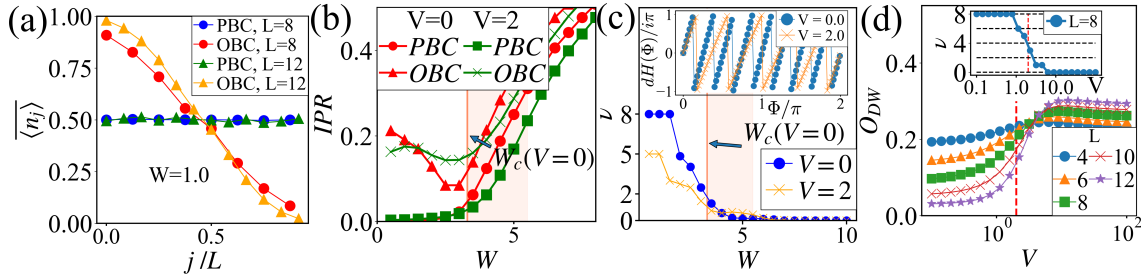
Under the PBC, the model exhibits a complex-real transition of the eigenenergy at $W = W_c = 2e^g$; here, we switch off the inter-particle interaction: $V = 0$ for the moment. Concomitantly, the corresponding wave function shows a delocalization-localization transition at the same value of $W = W_c$. Under the OBC, the eigen wave functions shows a peculiar damping, or an exponential decay in the regime of weak disorder (Fig. 1 (a)); this is often called non-Hermitian skin effect. Under the PBC, the same parameter region corresponds to the regime of complex energy (Fig. 1 (d)) and delocalized wave function (Fig. 1 (c)). To quantify these issues, we have here considered the inverse participation ratio (IPR): IPR $= \sum_j |\psi_j|^4$ as a measure of the localizability of the wave function $\psi_j$. Note that for a delocalized wave function IPR $\simeq 0$ (vanishes as $\simeq 1/L$, with $L$ being the size of the system), while for a localized wave function IPR $\simeq 1$; this includes the case of a wave function susceptible to the skin effect . Fig. 1 (a) shows the IPR under OBC in the space of parameters $(W, g)$. For a given $g$ one can observe that IPR $\simeq 1$ (skin effect is effective) in the regime of weak disorder, then it once diminishes (IPR $\simeq 0$) in the critical regime $W \sim W_c$, while in the regime of strong disorder: $W > W_c$ IPR increases again and takes a value $\simeq 1$. Fig. 1 (c) shows the corresponding behavior of IPR under PBC, in which IPR $\simeq 0$, i.e., the wave function is delocalized in the regime of weak disorder: $W < W_c$. Fig. 1 (d) shows the variation of the ratio $f_{\text{im}} = N_D/L$, where $N_D$ is the number of the eigenenergy which has $Im(|\epsilon|) > 10^{-13}$ in the same space of parameters $(W, g)$. In the delocalized phase, most of the eigenenergies are complex: in contrast, in the localized phase, eigenenergies become real, i.e., the delocalization-localization transition accompanies the complex-real transition.

In Fig. 1 (b) a topological interpretation [5] is given to the skin effect. For that a winding number $\nu$ that counts how many times the (complex) spectrum under PBC winds arounds the origin in the complex energy plane as the crystal momentum $k$ once goes around the Brillouin zone. In the presence of disorder (quasi-periodic potential), or in case of the broken translational symmetry, we introduce a flux $\Phi$ that twists the periodic boundary condition and plays the role of $k$ in this case; the winding number $\nu$ is then given as

$$\nu = \int_0^{2\pi} \frac{1}{2\pi i} d\Phi \partial_\Phi \log \det[H(\Phi) - E_0], \tag{3}$$

where $E_0$ is the base energy, which we choose here as $E_0 = 0$. In the practical calculation, we also employ a finite difference instead of the differential in Eq. 3; $\nu$ is calculated by collecting finite differences of $H(\Phi)$ in 201 points ($d\Phi = \frac{2\pi}{201}$). Fig. 1 (b) the distribution of $\nu$ in the parameter space

$(W, g)$ is shown and compared with the behavior of other indices: panels (a), (c), (d). They all suggest that the transition occurs at $W = W_c = 2e^g$.
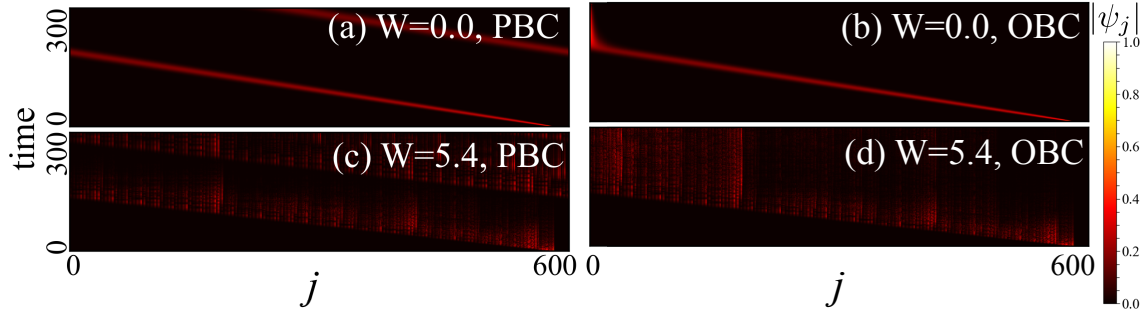


**Fig. 2.** Static properties (many-particle case): (a) local density $\langle n_j \rangle$ under OBC and PBC, (b) $\mathcal{IPR}$ as a function of the disorder strength $W$, (c) the winding number $\nu$ as a function of $W$. 50 disorder realizations. All eigenstates averaged. Inset of the panel (c) shows $dH(\Phi)$ as a function of $\Phi$ with W=0.5 and $\theta_0 = 0$. The shaded region indicate the crossover regime; $W_c$ is now renormalized by $V$. (d) Charge density-wave order parameter $O_{DW}$ of ground state (under OBC) as a function $V$. The red dashed line locates $V = 2$. Inset shows the winding number $\nu$ as a function of $V$ with W=0 and $\theta_0 = 0$.

In the case of a single particle we have seen so far all the eigenstates under the OBC tend to be localized exponentially toward an end of the system, and perhaps in an extreme case, localized to a single site at the boundary. Four panels of Fig. 2 show that the above single-particle scenario holds also true in the many-particle case; here we consider the case of $N = L/2$ particles (half-filling). Fig. 2 (a) shows the distribution of the local density $\langle n_j \rangle = \langle \mu | n_j | \mu \rangle$ for $L = 8, 12$, where the label $\mu$ specifies a many-body eigenstate. Under the OBC, $\langle n_j \rangle$ exhibits an asymmetric density profile; particles are predominantly located on the left half of the system. In this "many-body skin effect" [6], particles are only moderately localized to one end of the system as a consequence of the competition between the asymmetry in hopping and the Pauli exclusion principle that prohibits all skin modes located at the same site. The corresponding value of the many-body IPR [Fig. 2 (b)], defined as $\mathcal{IPR} = \sum_{\{n\}} |c_{\{n\}}|^4$, is indeed smaller than the one for the single-particle skin effect [cf. Fig. 1 (a)]; $|\mu\rangle = \sum_{\{n\}} c_{\{n\}} |\{n\}\rangle$, and $|\{n\}\rangle$ represents a computational basis. $\mathcal{IPR}$ measures a localization tendency in the many-body Fock-space. Fig. 2 (b) reveals a different behavior of $\mathcal{IPR}$ under PBC vs. OBC. With the increase of disorder strength $W$ $\mathcal{IPR}$ shows under the OBC a dip in the critical regime: $W \sim W_c$, before it turns to increase in the MBL regime. Under the PBC, $\mathcal{IPR}$ stays $\simeq 0$ until it surges after a critical disorder strength $W = W_c$. This is consistent with the behavior of the many-body winding number $\nu$ [Fig. 2 (c)], defined as Eq. 3 (inset shows typical behavior of $dH(\Phi)$). Non-zero $\nu$ corresponds to the appearance of many-body skin modes [7]. Note that $\nu$ is not the number of skin mode.

Here, our main focus is on the excited states of the Hatano-Nelson model, but it is also interesting to investigate the properties of the ground state; we assume the OBC case with real eigen-energies. Fig.2 (d) shows the change of charge density-wave order parameter $O_{DW} = \frac{1}{L} |\sum_i (-1)^i \langle n_i \rangle|$ in the ground state ($W = 0$) as a function of the inter-particle interaction V. $O_{DW}$ sharply increases at $V = 2$, i.e., many-body skin mode disappears and the CDW order emerges. Recently, Ref. 8 has reported that a strong interaction prohibits quantum states to thermalize, realizing a feature of Fock-space fragmentation. It is indeed interesting to study how many-body skin modes are suppressed by the inter-particle interaction $V$. In the inset of the Fig. 2(d) we show that (the change of) the behavior of $O_{DW}$ is concomitant with the vanishing of a finite winding number $\nu$.

## 3. Dynamical properties

Let us turn our eyes to the dynamics of the system, and follow how an initial wave packet in our system evolves in time. The motivation to study the dynamics in a system described by a non-

**Fig. 3.** Single-particle dynamics. Evolution of a wave packet initially located at $j = j_0 = 580$. Comparison of different boundary conditions: PBC vs. OBC. (a), (b): clean limit ($W = 0$). (c), (d): critical disorder regime ($W = 5.4 \sim W_c$). $M = 15$, $\delta t = 0.2$; see sec. 3.3 for details.

Hermitian Hamiltonian such as the one given in Eq. (1) may be two-fold. On one hand, a system effectively well described by such a non-Hermitian Hamiltonian emerges dynamically, i.e., as a non-equilibrium situation, e.g., realized in an open quantum system. On the other hand, to study the quantum dynamics resulting from a non-Hermitian Hamiltonian with the peculiar properties outlined in the previous subsection, such as the complex spectrum, the wave function showing skin effect, etc. is *per se* of much interest, resulting in a number of insightful findings.

### 3.1 The wave-packet dynamics: single-particle case

We choose the initial wave packet to be the one localized at site $j = j_0$: $|\psi(t = 0)\rangle = |j_0\rangle$. At time $t$, the wave packet may evolve as

$$|\psi(t)\rangle = \sum_j \psi_j(t)|j\rangle = \sum_n c_n e^{-i\epsilon_n t}|n\rangle, \tag{4}$$

where $|n\rangle$ represents the $n$th single-particle eigenstate of the Hamiltonian (1) with an eigenenergy $\epsilon_n$; i.e., $H|n\rangle = \epsilon_n|n\rangle$, while $c_n = \langle\langle n|\psi(t = 0)\rangle$. Here, $\langle\langle n|$ represents the left eigenstate corresponding to the eigenenergy $\epsilon_n$: $\langle\langle n|H = \epsilon_n\langle\langle n|$ and not $|n\rangle^\dagger$; $\langle\langle n| \neq |n\rangle^\dagger$. Note that the left and right eigenstates satisfy the biorthogonal condition, $\langle\langle n|m\rangle = \delta_{n,m}$. This biorthogonality is another peculiarity of the non-Hermitian system.

We have seen in the last section that in case of $g \neq 0$ $\epsilon_n$ becomes complex under the PBC in the regime of weak $W$. Eq. (4) implies that those eigenstate with large Im $\epsilon_n$ becomes dominant in the time evolution, and eventually $|\psi(t)\rangle$ converges to an eigenstate with the maximal Im $\epsilon_n$. This makes the time evolution non-unitary. In the simulation shown below, we, therefore, renormalize $|\psi(t)\rangle$ as $|\psi(t)\rangle \rightarrow |\tilde{\psi}(t)\rangle = |\psi(t)\rangle/\sqrt{\langle\psi(t)|\psi(t)\rangle}$. In the Hermitian case ($g = 0$) an equal superposition of different eigenstates and their quantum interference in the time evolution leads to spreading of the wave packet. Here, in case of $g \neq 0$ such quantum interference of the eigen wave function is strongly suppressed. As a result, the wave-packet dynamics becomes pseudo-classical, and the probability density $|\psi_j(t)|^2$ obeys effectively the classical diffusion equation, at least, as in the non-Hermitian case [9] (Fig. 3 (a)). Instead, the wave packet simply slides , reflecting the uni-directionality of the model (asymmetry of the hopping); in this sense this is a natural result. Under the OBC, $\epsilon_n$ is no longer complex but real. Still, the behavior of the time evolution is indistinguishable from the case of PBC (Fig. 3 (b)), until the wave packet reaches the boundary; in case of OBC, a mechanism different from the one for PBC is responsible for the apparently same time evolution. From the outset, it is rather natural that a local dynamics of a wave packet, here, in question, is insensitive to the boundary condition.

Effects of disorder (case of $W \neq 0$) is also very different from the Hermitian case. In the Hermitian case, disorder suppresses spreading of the wave packet, since it weakens the quantum interference.

Here, in case of $g \neq 0$, disorder, on the contrary, enhances spreading of the wave packet (Fig. 3 (c)). In the critical regime $W \simeq W_c$, a cascade-like enhancement of the wave packet spreading is conspicuous (Fig. 3 (c) and (d)).
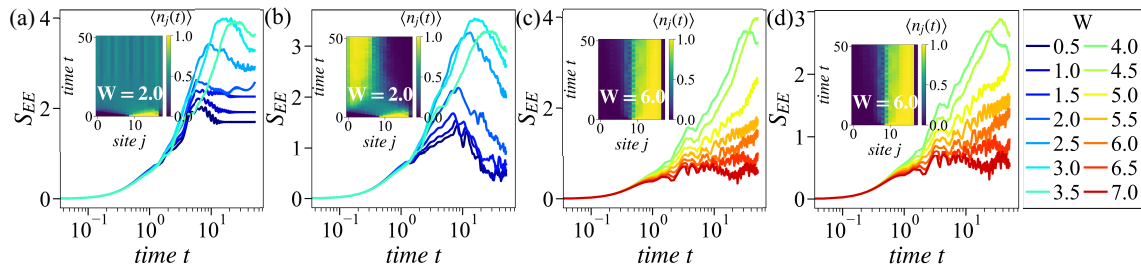
### 3.2 Many-particle case: density and entanglement dynamics

Here, we extend the analysis in the previous subsection on the wave-packet dynamics in the single-particle case to many-particle systems. We have studied an entanglement entropy $S_{EE}$ defined as $S_{EE}(t) = -\operatorname{Tr}\rho_R \ln\rho_R$, where $\rho_R = \operatorname{Tr}_L |\Psi(t)\rangle\langle\Psi(t)| = \sum_{L,R_1,R_2} \psi_{L,R_1}\psi_{L,R_2}^* |L,R_1\rangle\langle L,R_2|$ is a reduced density matrix ($L$ and $R_i$ define left and right half of system in the real space, respectively) calculated by traceing out the left half of the system. Here, we consider the case of $N = L/2$ particles in a system of size $L$ (half-filling), and choose the initial state to be the following domain wall state:

$$|\Psi(t = 0)\rangle = |00\cdots011\cdots1\rangle, \tag{5}$$

i.e., the last $L/2$ sites are occupied.

Four panels of Fig. 4 show some typical examples of the dynamics for the initial state (5) for $g = 0.5$ and for different values of disorder strength $W$. The dynamics of the density $n_j(t)$ is shown in the insets. In the regime of weak disorder (Fig. 4 (a) and 4 (b)) the system is in the delocalized phase, so that the initial domain wall structure tends to dissolve into a uniform distribution in the case of PBC (Fig. 4 (a), inset). Correspondingly, the entanglement entropy $S_{EE}(t)$ increases as $t$ increases, while in the regime of long time scale $t \sim 10^1$, it turns to decrease, resulting in a non-monotonic evolution of $S_{EE}(t)$. Recall that an initial quantum state is generally a superposition of the eigenstates with an individual phase factor, as time passes by, they tend to behave like a random vector; thus increasing the entanglement entropy $S_{EE}(t)$ [10]. However, in this regime, the eigenenergies are complex, so that as time evolves, such a superposition tends to be lost, i.e., $|\Psi(t)\rangle$ converges to eigenstate with maximal imaginary eigenenergy (here we name the eigenstate as $|R_{max}\rangle$), and the entanglement entropy $S_{EE}(t)$ turns to decrease. Such a convergence process appears as a plateaux of the $S_{EE}(t)$ after certain time.



**Fig. 4.** Typical entanglement dynamics: (a) delocalized phase with PBC, (b) delocalized phase with OBC, (c) localized phase with PBC, (d) localized phase with OBC. Inset of the each panel show time-evolution of the density pattern. $M = 25$, $\delta t = 0.05 - 0.2$; see sec. 3.3 for details. 5 disorder realizations. $L = 18$, $N = 8$, and $V = 2.0$.

Under the OBC [Fig. 4 (b)], $|\Psi(t)\rangle$ does not converge to $|R_{max}\rangle$ by complex spectrum because eigenenergy is real spectrum but realizing dynamics is still non-unitary due to non-orthogonality of the eigenvector ($\langle R_\nu|R_\mu\rangle \neq \delta_{\nu\mu}$), and $|\Psi(t)\rangle$ converges to $|R_\nu\rangle$, i.e., many-body skin mode. Interestingly, entanglement entropy $S_{EE}(t)$ still shows a non-monotonic evolution even though eigenenergies are real in this case. This occurs in a dynamical process of the many-body skin effect; here, starting with the initial configuration (5), particles tend to slide to the preferred direction, and after certain time they are relocated to their "right" positions prescribed by the many-body skin effect.

In the delocalized regime, both under PBC and OBC [Fig. 4 (a) and (b)], the $S_{EE}(t)$ increases with the increase of disorder strength $W$. This is due to the increase of scattering amplitudes by the quasi-periodic/disorder potential (2), which scatters a quasiparticle with crystal momentum $k$ to $k \pm 2\pi\theta$. As seen in the single-particle case, such the scattering gradually makes uni-directional dynamics cascade-like which leads quasiparticles to be more correlated with each other than free particle case; therefore, $S_{EE}(t)$ increases.

In the regime of strong disorder [Fig. 4 (c) and (d)] the density profile shows a clear localized feature, while the $S_{EE}(t)$ shows a logarithmic growth [11] . Practically, no dependence on the boundary condition : PBC vs. OBC.

### 3.3 Remarks on numerics

Here, to deal with a system of larger size than the ones in Ref. 9, we have employed the Krylov subspace method for non-Hermitian systems [12]. Since we focus on the time-evolution driven by a non-Hermitian Hamiltonian, we use the Arnoldi method instead of the Lanczos method to generate an orthonormal Krylov space $V_M$ from the Krylov space $K_M = span(|\Psi(t)\rangle, H|\Psi(t)\rangle, \cdots, H^{M-1}|\Psi(t)\rangle)$. Using $V_M$, a unit vector $|e_1\rangle = (1, 0, \cdots, 0)^T$ and $\tilde{H} = V_M^\dagger H V_M$, the time evolution of the quantum state is written as

$$|\Psi(t + \delta t)\rangle \sim V_M e^{-i\delta t \tilde{H}} V_M^\dagger |\Psi(t)\rangle = V_M e^{-i\delta t \tilde{H}} |e_1\rangle. \tag{6}$$

The advantage of this method is that the computational complexity of diagonalizing the Hamiltonian is reduced to that of diagonalizing a smaller $M \times M$ matrix $\tilde{H}$.

In the numerical calculation, we have employed QuSpin [13] for creating the non-Hermitian matrix such as the one given in Eq. (1).

## 4.  Concluding remarks

We have studied the static and dynamical properties of a non-Hermitian system, here, taking the Hatano-Nelson type model as a concrete example. Unlike the static properties sensitive to the boundary condition; e.g., complex vs. real spectrum, skin effect, etc., the dynamical properties are shown to be, apart from the effect of particle reaching the boundary, not particularly sensitive or insensitive to the boundary condition. We have observed the non-monotonic time evolution of the $S_{EE}(t)$ and its enhancement by disorder both under PBC and OBC. They have been interpreted as an interplay of disorder and non-Hermicity. There, such features as skin effect and the imaginary eigenenergy specific to the non-Hermitian system played a crucial role. In a future work, we will attempt a more systematic description of such unique entanglement dynamics in non-Hermitian systems.

### References
[1]  P. W. Anderson, Phys. Rev. **109**, 1492 (1958)
[2]  N. Hatano and D. R. Nelson Phys. Rev. B **56**. 8651 (1997)
[3]  S. Yao and Z. Wang, Phys. Rev. Lett. **121**, 086803 (2018)
[4]  S. Aubry and G. André, Ann. Israel Phys. Soc. **3**, 133 (1980)
[5]  Z. Gong, et al. Phys. Rev. X, **8**, 031079 (2018)
[6]  F. Alsallom, et al. Phys. Rev. Research **4**, 033122 (2022)
[7]  K. Kawabata, et al. Phys. Rev. B **105**, 165137 (2022)
[8]  G. D. Tomasi, et al. Phys. Rev. B **100**, 214313 (2019)
[9]  T. Orito, and K.-I. Imura, Phys. Rev. B **105**, 024303 (2022)
[10]  R. Nandkishore, and D. A. Huse, Annu. Rev. Condens. Matter Phys. **6**, 15 (2015)
[11]  M. Serbyn, et al. Phys. Rev. Lett. **110**, 260601 (2013)
[12]  Y. Saad, SIAM J. Numer. Anal. **29**, 209 (1992)
[13]  P. Weinberg and M. Bukov, SciPost Phys. **2**, 003 (2017); ibid. **7**, 20 (2019)